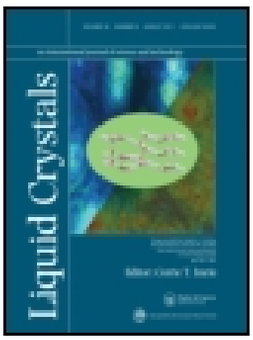

Liquid Crystals

ISSN: 0267-8292 (Print) 1366-5855 (Online) Journal homepage: http://www.tandfonline.com/loi/tlct20

Structure formation in monolayers composed of hard bent-core molecules

Paweł Karbowniczek, Michał Cieśla, Lech Longa & Agnieszka Chrzanowska

To cite this article: Paweł Karbowniczek, Michał Cieśla, Lech Longa & Agnieszka Chrzanowska (2016): Structure formation in monolayers composed of hard bent-core molecules, Liquid Crystals

To link to this article: http://dx.doi.org/10.1080/02678292.2016.1259510

Published online: 05 Dec 2016.

LIQUID CRYSTALS, 2016
http://dx.doi.org/10.1080/02678292.2016.1259510

Taylor & Francis
Taylor & Francis Group

INVITED ARTICLE

Structure formation in monolayers composed of hard bent-core molecules

Paweł Karbowniczek[a], Michał Cieśla[b], Lech Longa[b] and Agnieszka Chrzanowska[a]

[a]Institute of Physics, Cracow University of Technology, Kraków, Poland; [b]Marian Smoluchowski Institute of Physics, Department of Statistical Physics and Mark Kac Center for Complex Systems Research, Jagiellonian University, Kraków, Poland

ABSTRACT

We investigate the role of excluded volume interactions instabilising different structures in monolayers filled with bent-shaped molecules using the Onsager type of density functional theory supplemented by constant-pressure Monte-Carlo simulations. We study influence of molecular features, like the apex angle, thickness of the arm and the type of the arm edges on the stability of layered structures. For simple molecular shapes taken the observed phases are dominated by the lamellar antiferroelectric type as observed experimentally, but a considerable sensitivity of the ordering to details of the molecular shape is found for order parameters and wave vectors of the structures. Interestingly, for large opening angles and not too thick molecules, a window of stable nematic splay-bend phase is shown to exist.

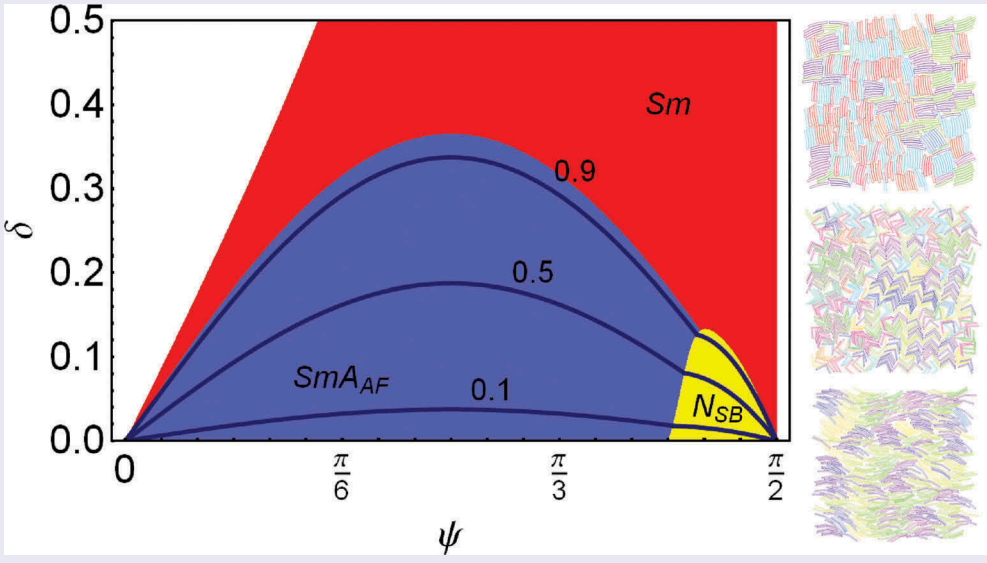

ARTICLE HISTORY
Received 24 May 2016

KEYWORDS
DFT of liquid crystals; perfect order approximation; MC simulations; smectics; nematic splay-bend

1. Introduction

Two-dimensional (2D) structures made by complicated macromolecules are recently of great interest due to their potential applications, mainly in photoelectronic and biosensor area [1–8]. In contrast to assemblies of spherical objects like, for instance, colloidal or nanosilica spheres, in case of anisotropic or irregularly shaped particles, there is a possibility to realise monolayers exhibiting very regular patterns which, next, can be utilised as a matrix capable to orient liquid crystal or to fabricate elements of electronic devices [5]. It has also turned out that the structure of a matrix built within a monolayer may influence the activity of biomolecules. This biomolecular effect is a first step for biosensors construction. A comprehensive and detailed report about ordered molecular assemblies formed by Langmuir–Blodgett films and self-assemblies with potential influence on biosensing capabilities is given in [2].

Achiral bent-core (banana)-shaped molecules can be important in this regard [1,3–5,9,10]. Their significance arises from the observation of extraordinary self-organisation in these mesogens in 3D, like the twist-bend nematic phase of nanoscale pitch [11,12], the fibre-

CONTACT Michał Cieśla michal.ciesla@uj.edu.pl Marian Smoluchowski Institute of Physics, Department of Statistical Physics and Mark Kac Center for Complex Systems Research, Jagiellonian University, ul. Łojasiewicza 11, Kraków 30-348, Poland

forming smectic twist-bend phase [13] and the cybotactic nematic phase [14]. They are also promising candidates to form the elusive biaxial nematic phase [15], the splay-bend nematic phase (N_{SB}) [16–19] and even more complex structures with tetrahedratic order [20–23].

In 2D, the situation is more subtle. These systems are generally characterised by the lack of true long-range order in the nematic state, which is a consequence of director fluctuations. A continuous nematic–isotropic phase transition goes here via Kosterlitz–Thouless disclination unbinding mechanism yielding what is observed as algebraically decaying orientational pair correlation function in the nematic phase [24]. It is observed, for example, in simulations of a 2D system of hard needles with zero thickness [25,26], for planar hard rods [27] and for zigzag and bow-shaped hard needles [28]. Even though the true long-range nematic order does not exist in these systems on a macroscopic scale, the simulations show that it persists over large spatial dimensions (*i.e.* on a mesoscopic scale). Interestingly, it can be well described by means of Onsager's density functionaltheory (DFT) [29–32], despite the fact that macroscopic fluctuations of the director are generally not included in DFT.

On the experimental side, the data of Gong and Wan [1] for banana-shaped liquid crystal molecules (P-n-PIMB) deposited on a highly orienting pyrolytic graphite (HOPG) surface reveal that the nematic order can be nearly saturated over the sample. Using scanningtunnelling microscopy (STM), the authors observed here several antiferroelectric chiral and non-chiral lamellar structures. Antiferroelectric smectic order in dense 2D banana systems has been also discussed theoretically as prevailing in [33] by Bisi et al. based on the packing arguments and, later, by Gonzales et al. in the case of needle-like, infinitely thin boomerangs [34] and hockey stick-shaped molecules consisting of two line segments [35]. It has been also detected in zero-thickness zigzag and bow-shaped systems [28]. In addition, in [28,34,35], the authors have observed that upon increasing pressure, before the system attains antiferroelectric smectic A phase, a spatially non-uniform, bend-deformed polar domains with the overall zero net polarisation are being formed.

Understanding molecular self-organisation in thin layers of more realistic, *finite-thickness* bent-core molecules is an interesting theoretical issue. Since most studies on 2D systems are based on the particles exhibiting geometrical shapes like needles [25,31,32], hard discorectangles [36] or zigzag particles [37] interacting via hard-core potentials, we will also incorporate a model from this class (it will be discussed in detail later). Both types of approach – Monte-Carlo (MC) simulations and Onsager's DFT – give consistent predictions here. Of particular importance on the phase stabilisation are excluded volume effects due to primary molecular features of the particles. In the case of bananas, these features are: length and width of the arms and the apex angle. As it will be shown, the secondary features like the shape of the arm's end contribute to quantitative changes.

As already mentioned above, the DFT of Onsager's type has proven to give a good insight into qualitative features of the phases. One of the benefits of using the DFT scheme in connection with bifurcation and symmetry analyses is the fact that it allows to cover a broad range of cases giving clear directions for a more detailed study. The theory predicts the existence of the ordered mesophases with weakly first or second-order phase transitions in 2D systems, and hence cannot predict quasi long-range order (QLRO), which is characteristic for systems with a continuous broken symmetry. Even though the Onsager's DFT does not account for QLRO, it works surprisingly well for nonseparable, hard-body interactions [29–32]. Indeed, a comparison of the Onsager DFT with MC simulations suggest that the former theory is able to account for relevant features of molecular self-organisation [25,28–32,34,37].

The aim of the present paper is to investigate with the Onsager's DFT a possibility of structure formation in monolayers built from hard bent-core molecules of zero and finite thickness. In particular, we show that a change in molecular shape can have a profound effect on the properties and even stability of the structures. We mainly limit ourselves to the case of high orientational order, in agreement with experiment [1] and previous 2D studies [34], but supplement the DFT analysis with a fullMC simulations to support validity of the approximation used.

The paper is organised as follows: Section II presents the model and Section III introduces the Onsager's DFT formalism together with the appropriately identified order parameters, needed for the structure description of aligned boomerangs. Section IV gives the results of the bifurcation analysis for N_{SB} and lamellar structures. Section V provides exemplary phase diagrams obtained from the full minimisation for three different bent-core systems: hard needle-like bananas, finite thickness bananas with flat horizontal edges and finite thickness bananas with squared edges. Finally, in the last section, a summary is given together with the main conclusions.

2. Model

We are going to study molecular self-organisation in a 2D system of hard bent-core molecules of finite thickness. Three types of molecules will be studied: needle-like boomerangs, Figure (1(a)), finite thickness boomerangs with horizontally cut edges (HB), Figure (1(b)) and finite thickness boomerangs with squared edges (SB), Figure (1(c)).

The bent-core needles, which are the reference particles given in Figure (1(a)), are just two line segments of the length l joined at one end in such a way that they form the apex angle of 2ψ. To obtain a HB molecule, the line segments are replaced by rhomboids whose tilt angle conforms to the assumption that the edges are effectively horizontal as in Figure (1(b)). The SB molecules will differ from the HB molecules with respect to the shape of the arm edges, which in the SB case are squared. D describes here the arm's thickness.

We should add that we sought for several possibilities of introducing finite thickness to needle-like boomerangs. The SB molecules seem to be the most natural extension, whereas boomerangs with horizontally cut arms (the HB particles) are expected to attain a layered arrangement more easily. Indeed, for the HB systems, even close packing arrangements correspond to lamellar order with polarised layers. Importantly, for all three cases, the excluded areas can be calculated analytically.

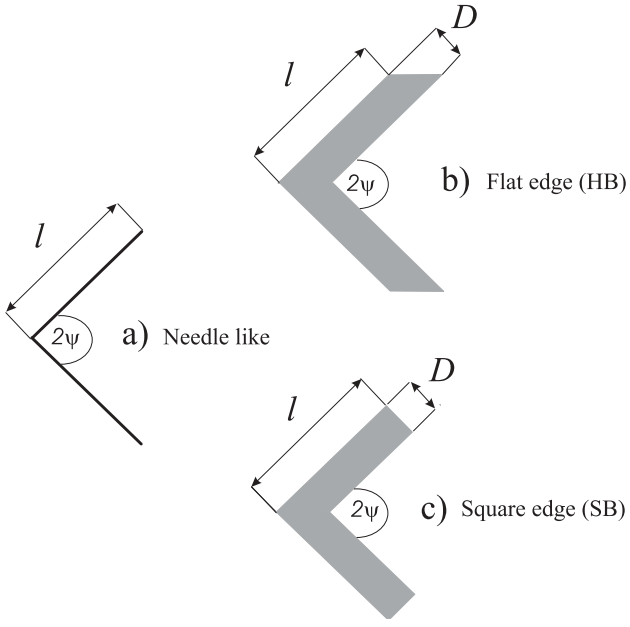

Figure 1. Shapes of bent-core molecules studied: (a) bent-core needles (they serve as a reference), (b) finite thickness bent-core molecules with flat horizontal edges (HB) and (c) finite thickness bent-core molecules with squared edges (SB). The apex angle, ψ, here is $\pi/4$ and the arm's width is $D = l/4$.

In order to compare the results for these three differently shaped bananas, Figure (1), we introduce the dimensionless shape parameter (width to arm's length ratio) $\delta = D/l$ $(0 \leq \delta \lesssim 1)$ and define the reduced density in agreement with one used for bent-core needles [34]

$$\rho = \bar{\rho} l^2 \sin(2\psi), \tag{1}$$

where $\bar{\rho} = N/S$ stands for the average density with N being the number of particles within the surface area S. Using definition of the packing fraction parameter $\eta = NS_{mol}/S$, with S_{mol} being the surface of the molecule, the reduced density becomes

$$\rho = \eta \frac{l^2 \sin(2\psi)}{S_{mol}}. \tag{2}$$

In the case of the HB particles, $S_{mol} = 2l^2\delta$. Thus,

$$\rho = \eta \frac{\sin(2\psi)}{2\delta}. \tag{3}$$

For the SB particles, $S_{mol} = l^2\delta(2 - \delta/\tan(\psi))$. Then,

$$\rho = \eta \frac{\sin(2\psi)}{\delta(2 - \delta/\tan(\psi))}. \tag{4}$$

Please note that the parameterisation (2) is singular for $\psi = 0$ and $\psi = \pi/2$, where bent-core molecules of zeroth thickness become reduced to a line, with $\eta = 0$. For 3D liquid crystals, the typical packing fractions accessible to liquid crystalline phases attain values from the interval (0.4–0.7). For 2D systems, including $\delta = 0$ case, η spans the whole interval (0–1). In particular, HB and SB boomerangs can reach their maximal possible value of $\eta = 1$ for ideal, close-packed, lamellar configurations with maximally polarised layers. Very high packing fractions for lamellar structures in 2D ($\eta \approx 0.8$) are also observed in the experiments of Gong and Wan [1].

3. Density functional analysis

3.1. Free energy functional and self-consistent equations

A successful approach to describe the phase behaviour of hard-body liquid crystalline systems is a generalisation of the Onsager theory. In this framework, the Helmholtz free energy, $\mathcal{F}$, is constructed as a functional of the single particle probability distribution function $P(X)$ [38]

$$\frac{\mathcal{F}[P]}{Nk_BT} = k_BT \underset{(X)}{Tr}\{\rho(X)[\ln(\Lambda\rho(X)) - 1]\} + \underset{(X)}{Tr}[\rho(X)V_{ext}] - \frac{k_BT}{2} \underset{(X_1,X_2)}{Tr}[\rho(X_1)f_{12}\rho(X_2)], \tag{5}$$

where

$$f_{12} = e^{-\beta V(X_1,X_2)} - 1 \tag{6}$$

is the Mayer function. Here, V is the interparticle potential, V_{ext} is the external potential, representing interaction with external fields, or surfaces, Λ is the constant resulting from the integration over momenta, T is the absolute temperature and k_B is the Boltzmann constant. $\rho(X)$ stands for the one-particle distribution function, which is normalised to the total number of particles N

$$\underset{(X)}{Tr}[\rho(X)] = \langle N \rangle \equiv N. \tag{7}$$

In what follows no external fields are taken into account and the surface is assumed smooth at the lengthscale of the molecular size (typically a fewnanometres for bent-core molecules). Its role is limited to confine molecules in 2D (strong planar anchoring). Under these assumptions, the corresponding V_{ext} does not depend on molecular orientational degrees of freedom and, hence, can be disregarded in the expansion (5).

The variable X represents the set describing the position $\mathbf{r} = (x, y)$ of the centre of mass of the particle and its orientations. In the description of lamellar structures we assume, in agreement with experiment [1] and previous 2D studies [34], that orientational order is nearly saturated. In practice it means that for a C_{2h}-symmetric molecule, the orientational degrees of freedom become reduced to a discrete variable, say s, accounting only for two possible orientations of the steric dipole ($s = \pm 1$) with respect to the *local* director $\hat{\mathbf{n}}(\mathbf{r})$, where $s = +1$ denotes a particle with a steric dipole pointing to the 'right' and $s = -1$ denotes a particle with a dipole pointing to the 'left'. This means that the steric dipole is assumed to stay perpendicular to the local director, Figure (2). In what follows we limit orientational degrees of freedom of a molecule to the above two values, but carry out exemplary NPT (constant number of particles, pressure and temperature) MC simulations with a full spectrum of translational and orientational degrees of freedom to check the credibility of this approximation. Hence, in 2D, the trace in Equations (5, 7) is calculated as

$$\begin{aligned} \underset{(X)}{Tr} = \sum_{s=\pm 1} \int_0^L dx \int_0^L dy = \\ \sum_{Md=L} S \sum_{s=\pm 1} \frac{1}{L} \int_0 dy, \end{aligned} \tag{8}$$

where L represents the linear dimension of our sample ($S = L^2$); M stands for the number of layers and d is the layer thickness in the case of smectics.

In order to obtain the equilibrium solutions for the distribution function, the free energy functional $\mathcal{F}[\rho]$ must be minimised with respect to variation of $\rho(X)$ subject to the normalisation constraint $\underset{(X)}{Tr}[\rho(X)] = N$. It amounts to minimising $\mathcal{F}^*[\rho]$ given by

$$\mathcal{F}^*[\rho] = \mathcal{F}[\rho] - \mu \left\{ \underset{(X)}{Tr}[\rho(X)] - N \right\}, \tag{9}$$

where μ is the chemical potential. In our case of ideally oriented hard boomerangs, the Mayer function has a meaning of an excluded distance. It reads

$$\begin{aligned} f_{12} &= e^{-\beta V(X_1,X_2)} - 1 \\ &= -\Theta[\xi(\hat{\mathbf{r}}_{12}, s_1, s_2) - r_{12}], \end{aligned} \tag{10}$$

where $\hat{\mathbf{r}}_{12} = \frac{\mathbf{r}_{12}}{r_{12}} = \frac{\mathbf{r}_2 - \mathbf{r}_1}{|\mathbf{r}_2 - \mathbf{r}_1|}$ and ξ is the contact function defined as the distance of contact from the origin of the second molecule for a given direction $\hat{\mathbf{r}}_{12}$ and orientations s_1, s_2 (see Figure (3)); Θ denotes the Heaviside function. Now, introducing the probability distribution function $P(X)$

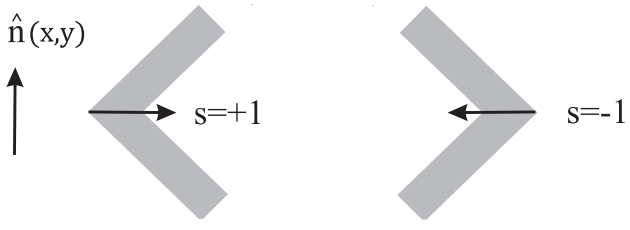

Figure 2. Definition of the s variable, accounting for different orientations of molecule's steric dipole with respect to the local director, $\hat{\mathbf{n}}(x, y)$.

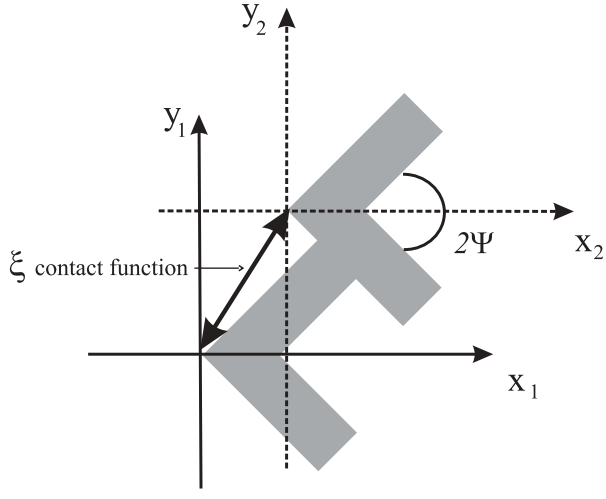

Figure 3. Definition of the contact function ξ for two molecules with the apex angle $2\psi = \pi/2$ and $\delta = D/l = 1/3$.

$$\rho(X) = NP(X) = \bar{\rho}SP(X) \tag{11}$$

and disregarding irrelevant (constant) terms, one can rewrite the free energy (5) in terms of a rescaled free energy per unit area, $f(P)$, as

$$\frac{f(P)}{l^2 \sin(2\psi)} = \frac{\beta\Delta\mathcal{F}[P]}{S} = \bar{\rho} \underset{(X)}{Tr}[P(X)\ln P(X)] + \frac{\bar{\rho}}{2} \underset{(X)}{Tr}\big[P(X)H_{eff}(X)\big], \tag{12}$$

where H_{eff} is the effective excluded volume, averaged over the probability distribution of particle '2'. It reads

$$H_{eff}(X_1) = \bar{\rho}S \underset{(X_2)}{Tr}\{P(X_2)\Theta[\xi(X_1, X_2) - r_{12}]\}. \tag{13}$$

The equilibrium distribution function is now obtained by minimising the free energy functional (12). The necessary condition reads

$$\frac{\delta f(P)}{\delta P} = 0, \tag{14}$$

which in practice becomes reduced to solving the self-consistent non-linear integral equations for $P(X)$

$$P(X) = Z^{-1}e^{-H_{eff}(X)}, \tag{15}$$

where

$$Z = \underset{(X)}{Tr}\, e^{-H_{eff}(X)} \tag{16}$$

is the normalisation of $P(X)$. The stationary solution of Equation (15) is denoted as $P_s(X)$.

3.2. Details of the calculation

In the analysis of possible stable phases, we disregard phases with 2D periodicity, like crystalline ones. Structures that are left are polar nematics, N_{SB} and commensurate or incommensurate smectics of A or C type, among which the most relevant are shown in Figure (4). Thus, for the case of perfectly aligned boomerangs only two variables are needed toparameterise one particle distribution function. For N_{SB}, we will assume the director to be a periodic function in x-direction, which means that $P(X) \equiv P(s, \hat{\mathbf{n}}(x))$, where $s = \pm 1$ represents two opposite orientations of the steric dipole with respect to the local director, Figure (4). For lamellar structures, we will use vertical coordinate y and s toparameterise P: $P(X) \equiv P(s, y)$. First, we will identify the bifurcation points from the perfectly ordered reference nematic phase.

For the cases not involving N_{SB} [16,17], the distribution function can be Fourier expanded as

$$P(s,y) = \tilde{A}_0 + \sum_{n=1}^{\infty} \tilde{A}_n \cos\left(\frac{2\pi n y}{d} - \phi_{0,n}\right) + s\tilde{B}_0 + \sum_{m=1}^{\infty} s\tilde{B}_m \cos\left(\frac{2\pi m y}{d'} - \phi_{1,m}\right), \quad 0 \le y \le L, \tag{17}$$

where periodic boundary conditions are assumed: $L = Md = M'd'$, with $M > 0$ and $M' > 0$ being integer numbers.

Note that the expansion (17) is the most general representation for $P(s, y)$, when particles are subjected to periodic boundary conditions and possible structures are characterised by positionally independent, homogeneous director field. It follows from the observation that $P(s, y)$, where $s = \pm 1$, is linear in s: $P(s, y) = \tilde{A}(y) + s\tilde{B}(y)$. Consequently, the independent Fourier expansions of $\tilde{A}(y)$ and $\tilde{B}(y)$ involve the density wave part ($\tilde{A}_n$-terms) and the polarisation wave part ($\tilde{B}_n$-terms) of periodicities d and d', respectively. They are phase-shifted with respect to each other (ϕ phases), where the phases are determined up to a global phase, expressing freedom in choosing the origin of laboratory system of frame.

Using orthogonality properties of the Fourier series and properties of the s-space, we can now define order parameters. They are given by

$$\begin{aligned} \langle x_n \rangle &= \langle x\left(\tfrac{2\pi n y}{d}\right)\rangle \\ \langle s x_m \rangle &= \langle s x\left(\tfrac{2\pi m y}{d'}\right)\rangle, \end{aligned} \tag{18}$$

where

$$\langle \ldots \rangle = \underset{(X)}{Tr}[P(X)\ldots] = S \sum_{s=\pm 1} \frac{1}{L} \int_0^{Md = M'd' = L} dy P(s,y)\ldots \tag{19}$$

with $x_\alpha \equiv \{c, s\}$ and, correspondingly, $x(\ldots) \equiv \{\cos(\ldots), \sin(\ldots)\}$. With definitions (18) we can finally rewrite the distribution function in the symmetry adapted form. It reads

$$P(s,y) = \tfrac{1}{2S} + \tfrac{1}{S}\sum_{n=1}^{\infty}\left[\langle c_n\rangle \cos\left(\tfrac{2\pi n y}{d}\right) + \langle s_n\rangle \sin\left(\tfrac{2\pi n y}{d}\right)\right] + \tfrac{1}{2S}\langle s\rangle s + \tfrac{1}{S}\sum_{m=1}^{\infty}\left[\langle s c_m\rangle s \cos\left(\tfrac{2\pi m y}{d'}\right) + \langle s s_m\rangle s \sin\left(\tfrac{2\pi m y}{d'}\right)\right]. \tag{20}$$

Substituting the expansion (20) back into the effective excluded volume (13) and assuming L to be large, we can reduce $H_{eff}(X_1)$ to a simpler form. It is given by

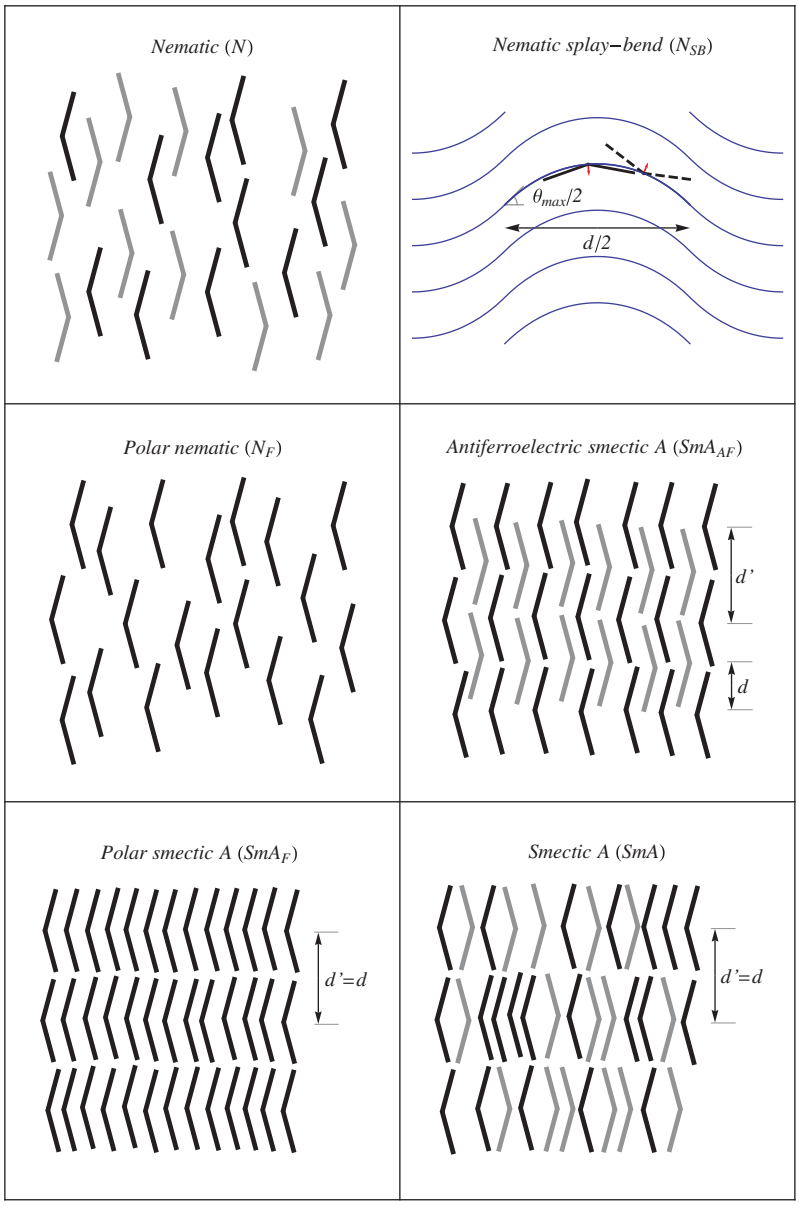

Figure 4. (Colour online) Possible arrangements of perfectly aligned bent-core molecules. For better visibility, the molecules pointing in opposite direction are drawn in different shades of grey. For the nematic splay-bend phase, which appears stable only for small δ, molecules are represented by thick continuous and dashed lines. The former corresponds to the most preferable orientation of the steric dipole (red arrow) with respect to the local director while the later is less preferable orientation. The director is tangential to the lines shown.

$$H_{eff}(X_1) = \bar{\rho} S \sum_{s_2=\pm 1} \int_0^L dy_2 \lambda(y_{12}, s_1 s_2) P(s_2, y_2), \tag{21}$$

where

$$\lambda(y_{12}, s_1 s_2) = \int_0^L \Theta[\xi(x_{12}, y_{12}, s_1 s_2) - r_{12}] dx_2 = \lambda_0(y_{12}) + s_1 s_2 \lambda_1(y_{12}) \tag{22}$$

plays the role of an excluded interval for fixed relative positions and orientations of two molecules.

This excluded area depends only on the relative orientation between the molecules and on their relative separation. There are two cases: with particles pointing in the same direction ($s_1 s_2 = 1$) or in the opposite direction ($s_1 s_2 = -1$). The exemplary cases are shown in Figure (5). For our molecules, the excluded area is calculated analytically, but only for the needle-like

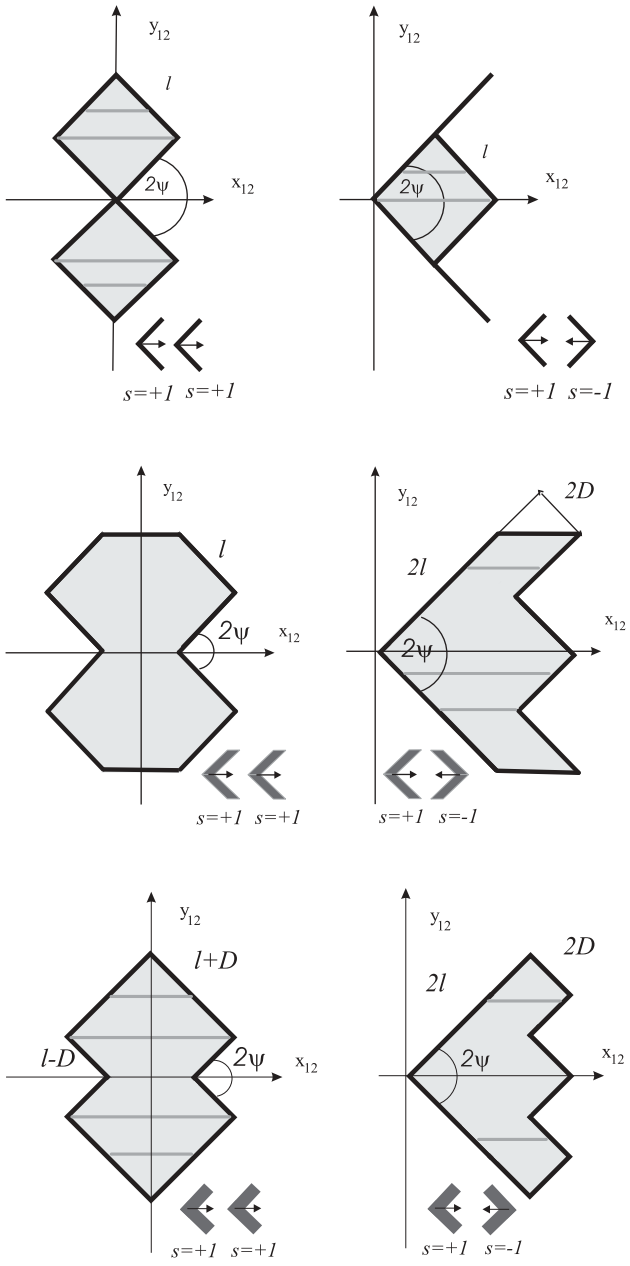

Figure 5. Excluded area in (x_{12}, y_{12}) plane for needle-like, HB and SB particles with $2\psi = \pi/2$ and $\delta = 1/3$. The grey areas correspond to the excluded areas, while the horizontal tie lines to the excluded distances.

bananas can the formulas be cast in a concise form. For $s_1 s_2 = 1$, they read

$$\begin{cases} -\frac{y_{12}+2l\sin\psi}{\tan\psi} \le x_{12} \le \frac{y_{12}+2l\sin\psi}{\tan\psi} & -2l\sin\psi \le y_{12} \le -l\sin\psi \\ \frac{y_{12}}{\tan\psi} \le x_{12} \le -\frac{y_{12}}{\tan\psi} & -l\sin\psi \le y_{12} \le 0 \\ -\frac{y_{12}}{\tan\psi} \le x_{12} \le \frac{y_{12}}{\tan\psi} & 0 \le y_{12} \le l\sin\psi \\ \frac{y_{12}-2l\sin\psi}{\tan\psi} \le x_{12} \le \frac{-y_{12}+2l\sin\psi}{\tan\psi} & l\sin\psi \le y_{12} \le 2l\sin\psi. \end{cases} \tag{23}$$

and for $s_1 s_2 = -1$

$$\begin{cases} x_{12} = -\frac{y_{12}}{\tan\psi} & -2l\sin\psi \le y_{12} \le -l\sin\psi \\ -\frac{y_{12}}{\tan\psi} \le x_{12} \le \frac{y_{12}+2l\sin\psi}{\tan\psi} & -l\sin\psi \le y_{12} \le 0 \\ \frac{y_{12}}{\tan\psi} \le x_{12} \le \frac{-y_{12}+2l\sin\psi}{\tan\psi} & 0 \le y_{12} \le l\sin\psi \\ x_{12} \le \frac{y_{12}}{\tan\psi} & l\sin\psi \le y_{12} \le 2l\sin\psi. \end{cases} \tag{24}$$

For needle-like boomerangs λs take a particularly simple form. They read

$$\lambda_0(y_{12}) = \begin{cases} l\cos\psi & |y_{12}| < l\sin\psi \\ \frac{-|y_{12}|+2l\sin\psi}{\tan\psi} & l\sin\psi \le |y_{12}| \le 2l\sin\psi, \end{cases} \tag{25}$$

$$\lambda_1(y_{12}) = \begin{cases} \frac{2|y_{12}|-l\sin\psi}{\tan\psi} & |y_{12}| < l\sin\psi \\ \frac{-|y_{12}|+2l\sin\psi}{\tan\psi} & l\sin\psi \le |y_{12}| \le 2l\sin\psi. \end{cases} \tag{26}$$

Examples of λs for needle-like boomerangs, HB and SB molecules are shown in Figure (6).

The next step is to perform the integration in (21) by replacing y_{12} with y, where $y_2 = y_1 + y$. In the limit of large L, the final formula for the effective excluded volume is given by

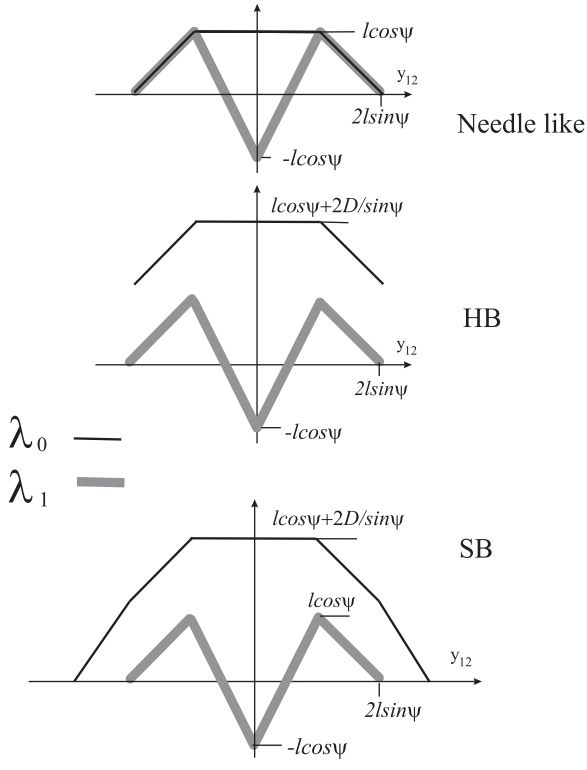

Figure 6. λ functions for needle-like boomerangs, HB and SB molecules. Coordinates of characteristic points of the functions are also given.

$$
\begin{aligned}
l^2 \sin(2\psi) H_{eff}(s_1, y_1) = \rho A_0 + \rho B_0 \langle s \rangle s_1 + \\
2\rho \sum_{n=1}^{\infty} \Bigg\{ \langle c_n \rangle \left[A_n \cos\left(\frac{2\pi n y_1}{d}\right) - C_n \sin\left(\frac{2\pi n y_1}{d}\right) \right] + \\
\langle s_n \rangle \left[A_n \sin\left(\frac{2\pi n y_1}{d}\right) + C_n \cos\left(\frac{2\pi n y_1}{d}\right) \right] \Bigg\} + \\
2\rho s_1 \sum_{m=1}^{\infty} \Bigg\{ \langle s c_m \rangle \left[B_m \cos\left(\frac{2\pi m y_1}{d'}\right) - D_m \sin\left(\frac{2\pi m y_1}{d'}\right) \right] + \\
\langle s s_m \rangle \left[B_m \sin\left(\frac{2\pi m y_1}{d'}\right) + D_m \cos\left(\frac{2\pi m y_1}{d'}\right) \right] \Bigg\},
\end{aligned}
\tag{27}
$$

where the coefficients of the expansion are defined as

$$
\begin{aligned}
A_n &= l^2 \sin(2\psi)\, \alpha(\psi, \delta, k_n) \\
&= \int_{-2l\sin\psi}^{2l\sin\psi} \lambda_0(y) \cos\left(\frac{2\pi n y}{d}\right) dy,
\end{aligned}
\tag{28}
$$

$$
\begin{aligned}
B_m &= l^2 \sin(2\psi)\, \beta(\psi, \delta, k'_m) \\
&= \int_{-2l\sin\psi}^{2l\sin\psi} \lambda_1(y) \cos\left(\frac{2\pi m y}{d'}\right) dy,
\end{aligned}
\tag{29}
$$

$$
\begin{aligned}
C_n &= l^2 \sin(2\psi)\, \gamma(\psi, \delta, k_n) \\
&= \int_{-2l\sin\psi}^{2l\sin\psi} \lambda_0(y) \sin\left(\frac{2\pi n y}{d}\right) dy,
\end{aligned}
\tag{30}
$$

$$
\begin{aligned}
D_m &= l^2 \sin(2\psi)\, \sigma(\psi, \delta, k'_m) \\
&= \int_{-2l\sin\psi}^{2l\sin\psi} \lambda_1(y) \sin\left(\frac{2\pi m y}{d'}\right) dy.
\end{aligned}
\tag{31}
$$

Here, ρ is defined in Equation (1) and k, k' are dimensionless wave vectors given by $k = \frac{\pi l \sin\psi}{d}$ and $k' = \frac{\pi l \sin\psi}{d'}$, respectively. As a result of the condition that $L = Md = M'd'$, we additionally have a limitation $Mk' = M'k$ imposed on wave vectors. Substitution of $n = m = 0$ in (28) and (29) gives A_0 and B_0.

Formally, the coefficients (28–31) are the Fourier transforms of λ_α, Equation (22). For the case of needle-like bananas, these coefficients are of a particularly simple form, namely

$$
\begin{aligned}
\alpha(\psi, \delta, 0) = \tfrac{3}{2},\ \beta(\psi, \delta, 0) = \tfrac{1}{2},\ \gamma(\psi, \delta, k) = \sigma(\psi, \delta, k) = 0, \\
\alpha(\psi, \delta, k) = \tfrac{[2\cos(2k)+1]\sin^2(k)}{2k^2}, \\
\beta(\psi, \delta, k) = \tfrac{[2\cos(2k)-1]\sin^2(k)}{2k^2},
\end{aligned}
\tag{32}
$$

where $k = \frac{l\pi \sin\psi}{d}$. They are shown in Figure (7).

Taking definitions (18) the non-linear integral Equation (15) becomes reduced to an infinite set of non-linear transcendental equations for the order parameters

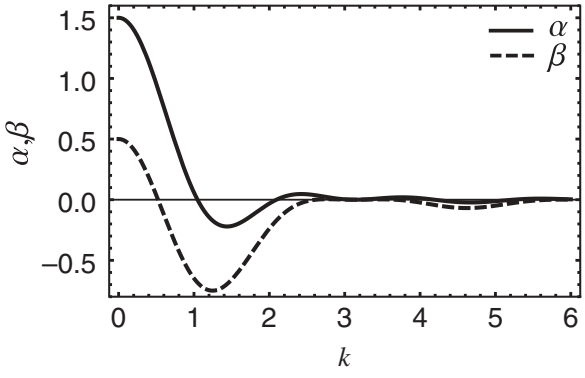

Figure 7. The k-dependence of the coefficients α and β for needle-like boomerangs.

$$
\begin{pmatrix} \langle x_n \rangle \\ \langle s x_m \rangle \\ \langle s \rangle \end{pmatrix} = Z^{-1} \underset{(X_1)}{Tr} \left[\begin{pmatrix} x\left(\frac{2\pi n y_1}{d}\right) \\ s_1 x\left(\frac{2\pi m y_1}{d'}\right) \\ s_1 \end{pmatrix} \exp(-H_{eff}) \right].
\tag{33}
$$

The corresponding stationary excess free energy in the limit of large L is given by

$$
\begin{aligned}
\frac{f[P_s]}{l^2 \sin(2\psi)} &= \bar{\rho} \langle \ln P_s \rangle + \tfrac{\bar{\rho}}{2} \langle H_{eff} \rangle = -\tfrac{\bar{\rho}}{2} \langle H_{eff} \rangle - \bar{\rho} \ln Z \\
&= -\tfrac{\bar{\rho}^2}{2} \Big[A_0 + B_0 \langle s \rangle^2 + 2 \sum_{n=1}^{\infty} A_n \left(\langle c_n \rangle^2 + \langle s_n \rangle^2 \right) \\
&\quad + 2 s_1 \sum_{m=1}^{\infty} B_m \left(\langle s c_m \rangle^2 + \langle s s_m \rangle^2 \right) \Big] - \bar{\rho} \ln Z.
\end{aligned}
\tag{34}
$$

Similar to the previous cases, we can now proceed with the analysis of N_{SB}. For the N_{SB} structure, we take the generalisation of one proposed earlier by Meyer [16]. Since the steric polarisation is always perpendicular to the local director, we assume the direction of the former to rotate uniformly between $-\theta_{max}/2$ and $\theta_{max}/2$ for $0 \le x < d/2$, Figure (4), where θ_{max} and d should be determined from the free energy minimum. Assuming the structure to be globally non-polar, we take

$$P(s,\hat{\mathbf{n}}(x)) = P(s,\hat{\mathbf{n}}(x+d)) = \frac{1}{2S} + \frac{1}{2S}\langle s\rangle s\delta[\hat{\mathbf{s}}(x) + \{\sin(\phi(x)),\cos(\phi(x))\}], \tag{35}$$

where

$$\phi(x) = \begin{cases} \frac{2\theta_{max}x}{d} - \frac{\theta_{max}}{2}, & 0 \le x < d/2 \\ \pi - \frac{2\theta_{max}x}{d} + \frac{3\theta_{max}}{2}, & d/2 \le x < d. \end{cases} \tag{36}$$

Here, $s\hat{\mathbf{s}}(x)$ is the local polarisation ($\hat{\mathbf{s}}(x)\perp\hat{\mathbf{n}}(x)$) with $s = \pm 1$, as previous, and $\delta[...]$ is the Dirac delta function. Note that the N_{SB} structure needs d, θ_{max} and the average polarisation $\langle s\rangle$ measured with respect to the local director to be determined variationally from the free energy $f[P_s]$. The calculation of the equations for $\langle s\rangle$ and for $f[P_s]$ proceeds in a similar way as previous. We only need to interchange y with x in formulas (21, 22, 33, 34), set $M = 1$ and disregard M'. The final formulas are identical to Equations (33, 34) with $A_n = B_n = 0$ for $n \ge 1$. The only difference now is that A_0 and B_0 depend on θ_{max} and d.

The Equation (33) should be solved for given d, d' and appropriately chosen M, M'. Then, the equilibrium structure is identified with the absolute minimum of (34) taken with respect to the stationary solutions and with respect to the periodicities d, d' and θ_{max}. Note that the trivial nematic state corresponding to $\langle s\rangle = \langle c_n\rangle = \langle s_n\rangle = \langle sc_n\rangle = \langle ss_n\rangle = 0$ ($\forall \cdot n$) always satisfies Equation (33). The remaining problem is to identify all non-trivial solutions of Equation (33), where at least one of the order parameters becomes non-zero. A systematic way of finding these solutions is bifurcation analysis [39]. Here, we apply this technique to analyse bifurcation from the nematic phase. We also determine exemplary phase diagrams from the fullminimisation of the free energy in different phases, over a wide range η. We also carry out exemplary MC simulations that involve a full spectrum of orientational degrees of freedom to support the usefulness of the ideal nematic order approximation.

3.3. Bifurcation analysis

Now we consider a bifurcation from a perfectly aligned nematic phase. Close to the bifurcation point, the difference between the states is arbitrarily small for each d, d', which enables one to linearise the right-hand side (RHS) of Equation (33) with respect to the order parameters. The analysis is carried out by taking the needle-like boomerangs as reference. The results are

$$\begin{pmatrix} \langle c_n\rangle \\ \langle s_n\rangle \end{pmatrix} = -\rho\mathbf{A}_n \begin{pmatrix} \langle c_n\rangle \\ \langle s_n\rangle \end{pmatrix}, \tag{37}$$

$$\begin{pmatrix} \langle sc_m\rangle \\ \langle ss_m\rangle \end{pmatrix} = -\rho\mathbf{B}_m \begin{pmatrix} \langle sc_m\rangle \\ \langle ss_m\rangle \end{pmatrix}, \tag{38}$$

$$\langle s\rangle = \rho\beta(0)\langle s\rangle, \tag{39}$$

where 2 by 2 arrays $\mathbf{A}_n$, $\mathbf{B}_m$ are given by

$$\mathbf{A}_n = \begin{pmatrix} \alpha(\psi,\delta,k_n) & \gamma(\psi,\delta,k_n) \\ -\gamma(\psi,\delta,k_n) & \alpha(\psi,\delta,k_n) \end{pmatrix} \tag{40}$$

and

$$\mathbf{B}_m = \begin{pmatrix} \beta(\psi,\delta,k'_m) & \sigma(\psi,\delta,k'_n) \\ -\sigma(\psi,\delta,k'_m) & \beta(\psi,\delta,k'_n) \end{pmatrix}. \tag{41}$$

The homogeneous Equations (37–39) have a non-trivial solution given that at least one of the equations

$$\det(1+\rho\mathbf{A}_n) = 0, \tag{42}$$

$$\det(1+\rho\mathbf{B}_m) = 0, \tag{43}$$

$$\rho \equiv \rho_0 = -\frac{1}{\beta(0)} \tag{44}$$

is satisfied for a positive ρ. By solving Equations (42, 43) for ρ, we obtain two functions: $\rho(k_n)$ and $\rho'(k'_m)$, respectively, together with ρ_0. The bifurcation density is then identified with the lowest positive value taken out of

$$\left\{ \underset{\{k_n\}}{\mathrm{Min}}[\rho(k_n)], \underset{\{k'_m\}}{Min}[\rho'(k'_m)], \rho_0 \right\}. \tag{45}$$

For the majority of cases studied, we will assume the director to be perpendicular both to the molecule's dipole moment and the layer normal, see Figure (2). In this case, $\lambda = \lambda(|y_{12}|, s_1 s_2)$ in Equation (22). Consequently, we can choose ϕs in Equation (17) to vanish and consider the case of vanishing $\langle s_n\rangle$ and $\langle ss_m\rangle$. The corresponding bifurcation density is then the lowest positive value out of

$$\left\{ \underset{\{k_n\}}{\mathrm{Min}}\left[\frac{-1}{\alpha(k_n)}\right], \underset{\{k'_m\}}{Min}\left[\frac{-1}{\beta(k'_m)}\right], \frac{-1}{\beta(0)} \right\}. \tag{46}$$

As an example, we start with the discussion of bifurcation for needle-like boomerangs. It turns out that the most stable structures bifurcating from the nematic phase is the antiferroelectric smectic A phase (SmA_{AF}). To see this, consider the behaviour of $\alpha(k_n)$ and $\beta(k'_m)$, shown in Figure (7). One observes that β attains the absolute minimum for $k'_{0,m} = 1.246$ and α for $k_{0,n} = 1.438$, and that these points correspond to the layer thicknesses of $d'_{0,m} = \frac{lm\pi\sin\psi}{k'_{0,m}} = 2.52ml\sin\psi$ and $d_{0,n} = \frac{ln\pi\sin\psi}{k_{0,n}} = 2.184nl\sin\psi$, respectively. Consequently, the physical bifurcation to the smectic A (SmA) phase should occur for $n = 1$ with $d_0 \approx$

$2.18l\sin(\psi) = 1.09(2l\sin(\psi))$ and bifurcation to the antiferroelectric smectic (SmA_{AF}) phase for $m = 1$ with $d_0 \approx 2.51\sin(\psi) = 1.26(2l\sin(\psi))$. Since the minimum of B_m is deeper, the expected lamellar phase bifurcating from the nematic phase will be of the antiferroelectric type. The value of this minimum determines the bifurcation density ($\rho_{bif} = -\frac{1}{B_1^{\min}}$). Then, the distribution function at the bifurcation point will take the form

$$P(s,y) = \frac{1}{2S} + \frac{1}{S}\langle sc_1\rangle s\cos\left(\frac{2\pi y}{2.52l\sin\psi}\right) + \ldots \tag{47}$$

4. Possible structures

In general, the most probable 2D structures that can be expected in boomerang systems are given in Figure (4). Here, the low-density phase, the nematic phase, can be of two types: the standard nematic phase (N) in which the same (on average) number of boomerangs is pointing to the right as to the left. When one type of orientation prevails ($\langle s\rangle \neq 0$), then one deals with the polar (ferroelectric) nematic (N_F). One may also expect that the N_{SB} phase ($\langle s\rangle \neq 0$, finite d, $0 < \theta_{max} \leq \pi$) should be at least locally stable. Upon an increase of density, a transition to a smectic phase, which is characterised by a regular modulation of the density profile due to presence of the layers, may occur. Three different smectic phases are plausible: the typical smectic A phase (SmA), where left and right-pointing particles are, on average, equally distributed ($\langle c_n\rangle \neq 0$), the ferroelectric smectic A phase (SmA_F) when the particles oriented in one direction overwhelm the number of the oppositely oriented particles ($\langle s\rangle \neq 0$, $\langle c_n\rangle \neq 0$, $\langle sc_n\rangle \neq 0$, $d = d'$), and the antiferroelectric smectic A phase (SmA_{AF}), in which the particles in subsequent layers have opposite orientations ($\langle sc_n\rangle \neq 0$, $\langle c_n\rangle \neq 0$, $d' = 2d$). Note that the period d' of the layers with particles of the same average orientation in the antiferroelectric phase is twice the smectic period d ($M = 2M' = 2$), whereas in the polar phase they attain the same value. The occurrence of such phases will depend on the structure of the particles themselves as well as on the density.

5. Boomerangs of arms with finite width

5.1. The HB molecules

The model of the needle-like boomerangs can be extended to the case when arms are of finite width in many different ways of which we choose HB and SB shapes. The HB case is given in Figure (1(b)). For HB molecules, the coefficients α and β are given by

$$\begin{aligned}
\alpha(\psi,\delta,k) &= \frac{[1+2\cos(2k)]\sin^2 k + \frac{4\delta}{\sin(2\psi)}k\sin(4k)}{2k^2},\\
\beta(\psi,\delta,k) &= \frac{[-1+2\cos(2k)]\sin^2 k}{2k^2},\\
\alpha(\psi,\delta,k\to 0) &= \tfrac{3}{2} + \frac{8\delta}{\sin(2\psi)},\\
\beta(\psi,\delta,k\to 0) &= \tfrac{1}{2}.
\end{aligned} \tag{48}$$

Note that the coefficient β here is exactly the same as in the case of the needle-like boomerangs. It turns out, however, that when the condition $\delta = 0.3654\sin(2\psi)$ is fulfilled, the minimum of α and the minimum of β attain the same value $\beta_{min} = \alpha_{min} = -0.749956$ (see Figure (8)). This condition provides a set of values for the parameters serving as a limiting case when the bifurcation from N to SmA or SmA_F is observed. Note that the close-packed structure for HB molecules is of the lamellar (smectic A) type with maximally polarised layers, but the direction of polarisation within the layer is doubly degenerate ($\hat{\mathbf{s}} = \pm\hat{\mathbf{x}}$).

Using the density of the form $\rho = \eta\frac{\sin 2\psi}{2\delta}$, one can now obtain the bifurcation diagram as given in Figure (9). The lines provide the condition where the normalised packing fraction η is equal to 0.1, 0.5 and 0.9. Similar to [34], the most common smectic phase obtained here is SmA_{AF}, given by the blue region. In the red region (Sm) of Figure (9), the bifurcation scenario leads to a single amplitude SmA structure ($\langle c_1\rangle \neq 0$). However, due to the coupling of $\langle c_1\rangle$ with $\langle s\rangle$ and $\langle sc_1\rangle$, the equilibrium lamellar structures with polarised layers, like SmA_F, are also possible. They can be stabilised as a result of a phase transition between two different lamellar structures and cannot be obtained by studying bifurcation from N. In this case, we would need to solve numerically the self-consistent Equations (33) for each structure separately and compare the free energies of the solutions.

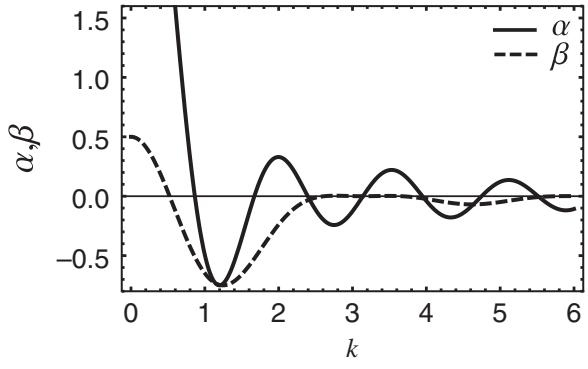

Figure 8. The Fourier transforms α and β for the condition $\delta = 0.3654\sin(2\psi)$.

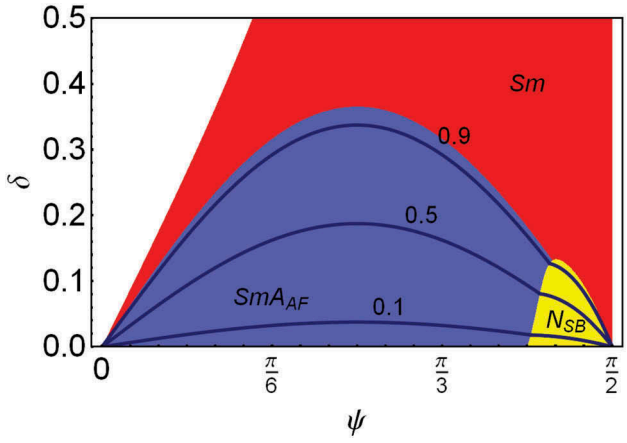

Figure 9. (Colour online) Bifurcation diagram for HB boomerangs. The blue region corresponds to the cases where nematic (*N*)-antiferroelectric smectic A (SmA_{AF}) bifurcation takes place and the red region (*Sm*) corresponds to the cases where the transition from *N* undergoes either to *SmA* or SmA_F. In the yellow region, the N_{SB} structure bifurcates from *N*. The black lines are the density limits with the packing fraction η given in the legend.

Interestingly, the theory predicts that the nematic splay-bend phase can be stabilised directly from *N* for not too thick molecules.

5.2. The SB molecules

In the case of the SB molecules, the calculation of the Fourier transforms for the excluded slice becomes more involved. Firstly, the particle width δ has to be smaller than $\tan(\psi)$ due to geometrical constraints. Secondly, three cases with different antiparallel arrangements (I, II, III) of the molecules (see Figure 10) have to be considered separately. The corresponding α and β functions entering the bifurcation equation, like those in Equation (48), should now be replaced by α_i and β_i $(i = I, II, III)$, respectively. The first two cases appear when the opening angle 2ψ is smaller than $\pi/2$. The first one of these

Figure 10. Three cases of antiparallel arrangements for SB molecules. They lead to three different Fourier transforms of the excluded slice given in Appendix.

two occurs also when arms are thin, namely when their width is smaller than $1/[\cot(\psi) + \csc(2\psi)]$. The corresponding normalised α_i and β_i functions for i = I, II, III are given in Appendix.

Examining the positions of relative minima for α_i and β_i (see Figure (11)), one observes bifurcations to different phases as shown in Figure (12). More specifically, the first panel of Figure (11) illustrates the case where the bifurcation to *SmA* or a transition to SmA_F takes place, which is connected with the coefficient α having a global negative minimum deeper than that of β. The next panel shows the opposite case,that is, when the (negative) global minimum of β is deeper than that of α, hence the bifurcating phase will be SmA_{AF}. When the (negative) global minima are about the same depth, we can expect an incommensurate smectic phase to become absolutely stable. Within our formalism, this case can be studied by taking a commensurate approximation, where both minima are approximated by an appropriate choice of k, k' and M, M'.

Similar to the HB case, the coefficient β at $k_m = 0$ is always positive, thus the polar nematic phase cannot appear here either. The complete bifurcation diagram is presented in Figure (12). The blue region in this

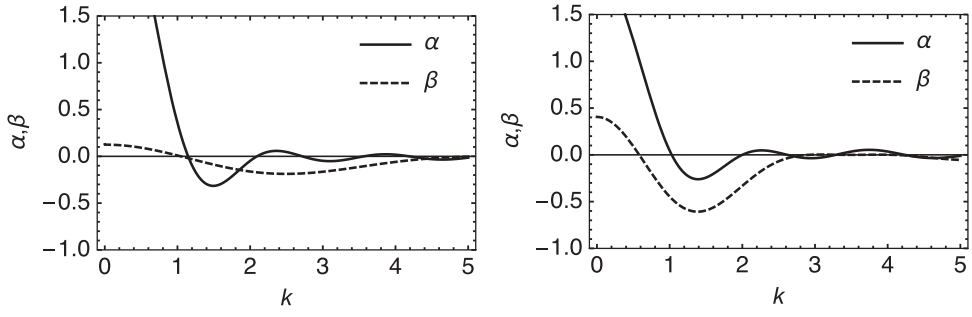

Figure 11. Different relations between absolute minimum of α and β. Left diagram corresponds to $\psi = \pi/4$ and $\delta = 0.5$ and bifurcation to smectic A phase. Right diagram corresponds to $\psi = \pi/4$ and $\delta = 0.1$, where bifurcation is to antiferroelectric smectic phase.

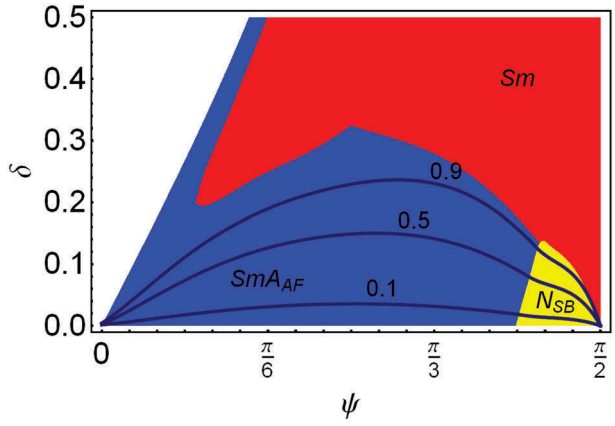

Figure 12. (Colour online) Bifurcation diagram for SB boomerangs. The blue region corresponds to the cases where nematic (*N*)–antiferroelectric smectic A (SmA_{AF}) bifurcation takes place and the red region corresponds to the cases where the nematic (*N*)–smectic A (*SmA*) or nematic (*N*)–polar smectic A (SmA_F) bifurcation undergoes. In the yellow region, N_{SB} bifurcates from *N*. The black lines are the density limits with the packing fraction η given in the legend.

diagram corresponds to the apex angle and arm thickness where the bifurcation from *N* to SmA_{AF} takes place. The red area (*Sm*) again corresponds to $N-SmA$ bifurcation or $N-SmA_F$ transition and in the yellow area the bifurcation is dominated by N_{SB}. The black lines are the guide lines at which the packing fractions are given as in the legend.

Finally, we would like to add that we have checked a few cases for the possibility of obtaining a stable incommensurate smectic phases of A type and a smectic C phase, where the director is not perpendicular to the layer normal, but did not find one more stable than the structures identified in Figures (9 and 12).

5.3. Nematic splay-bend

Both, HB and SB bifurcation diagrams contain previously described nematic splay-bend regions, but the range of stability of N_{SB} is narrow, starting from ψ around $5\pi/12$. Another limiting factor is the width δ of a particle, which cannot be greater than 0.14. In Figure (13), further characteristics of N_{SB} are shown. In particular, please note that the period *d* of N_{SB} increases with increasing opening angle, but the width of a particle has no significant effect on *d*. It only reduces the range of ψ at which the N_{SB} phase can occur. However, θ_{max} can be drastically altered by the width of a particle. For hard needles of $\psi = 5\pi/12$, it approaches its maximal value of π, which means that molecules perform a full half turn on the path of length $d/2$, but as the thickness of particles increases θ_{max} becomes smaller. The same effect is observed when the opening angle of molecules increases. It causes θ_{max} to decrease towards $\pi/2$, which means that the tilt angle of the director with respect to the *x*-axis varies between $\pi/4$ and $-\pi/4$.

Please remember that weparameterise our results using the convention adopted for bent-core needles [27]. As already mentioned before thisparameterisation is singular in the needle limit $\psi = 0, \pi/2$ due to the factor $l^2 sin(2\psi)$ in Equation (2), where bent-core molecules of zeroth thickness become reduced to a line. Therefore, any polar order that may occur for $\psi = \pi/2$ in Figures (9 and 12) is only asymptotically stable, for $\eta \to \infty$.

5.4. Exemplary results of full minimisation

Here, the free energy of different phases is calculated for exemplary molecular shapes to identify the stable phases as function of packing fraction. It turns out that for majority of cases the calculations involving terms up to $n = m = 4$ in (33) and (34) give excellent quantitative predictions for the equilibrium structures. The results obtained are consistent with the phase diagram maps, Figures (9 and 12), in apex angle–arm's width plane. Here, we concentrate on the most common

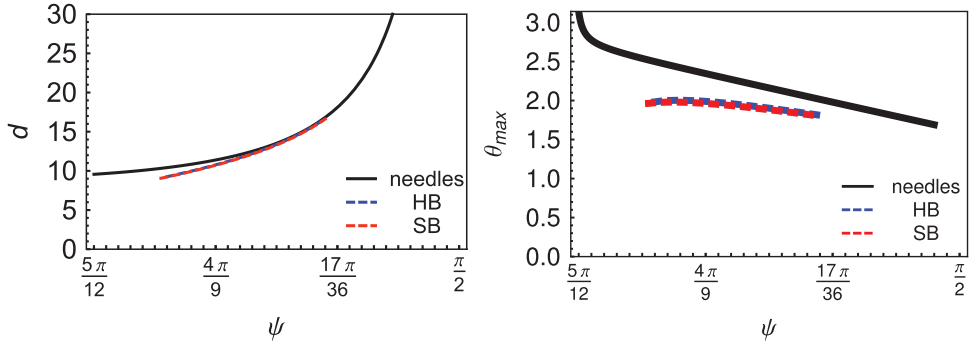

Figure 13. (Colour online) Behaviour of period *d* and θ_{max} as function of ψ for N_{SB} calculated at bifurcation from the nematic phase. Blue and red lines correspond to HB and SB particles of width $\delta = 0.1$.

SmA_{AF} phase and clarify the issue of previously mentioned SmA_F phase.

We start with the case of stable SmA_{AF}, represented by the blue region in Figures (9 and 12). In Figures (14 and 15), we compare the equilibrium values of leading order parameters for this structure as function of packing fraction and arm's width for $\psi = \pi/3$. It turns out that the change of the arm endings strongly influences the behaviour of the order parameters, especially when the thickness of the arms increases. As expected, for thin arms, where, for instance, $\delta = 0.05$, the profiles of the order parameters (and the bifurcation points) are very similar. For larger values of δ, the bifurcation point for the SB boomerangs shifts towards higher packing fractions. For $\delta = 0.25$, one does not observe the stable SmA_{AF} phase, whereas for the HB boomerangs this structure is still attainable.

In Figures (16) and (17), the equilibrium wave vector k of the SmA_{AF} phase, obtained for different packing fractions η and the apex angle of $2\psi = 2\pi/3$ and $2\psi = 2\pi/4$, respectively, is presented for HB and SB molecules. In case of HB molecules, the k vector increases with the packing fraction, which means a reduction of the layer thickness. For the SB molecules, the wave vector k can show different behaviour. In the case of $2\psi = 2\pi/3$, for thicker arms (δ>0.15), the wave vector is reduced with the packing fraction and hence the layer thickness increases.

In order to determine the sequence of phase transitions and establish relations between them in the red (Sm) regions of the bifurcation diagrams, we compared the free energies for the reference structures using the first terms in Equations (33) and (34), and then calculated the order parameters up to $n = m = 4$. The results showing stable SmA and SmA_F phases are shown in Figures (18) and (19) for two HB systems: near ($\delta = 0.4$, $\psi = \pi/4$) and far ($\delta = 0.5$, $\psi = \pi/4$) from the blue region. For the cases studied the first

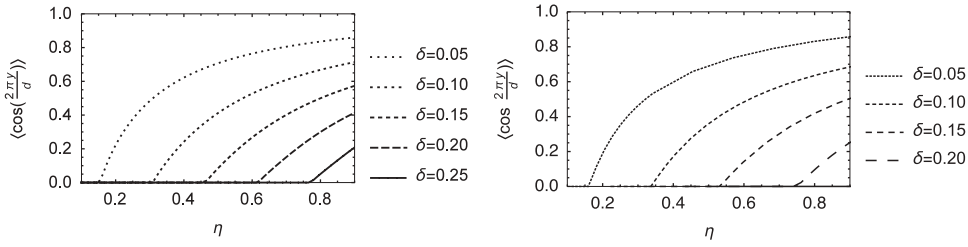

Figure 14. Typical behaviour of equilibrium order parameter $\langle c \rangle$ for the cases with stable SmA_{AF} phase, obtained for different packing fractions η and the apex angle $2\psi = 2\pi/3$. The panel on the left is for the HB molecules while the panel on the right is for the SB molecules.

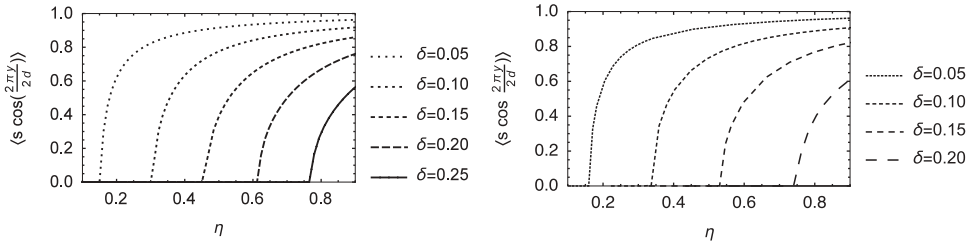

Figure 15. Typical behaviour of equilibrium order parameter $\langle sc \rangle$ for the cases with stable SmA_{AF} phase, obtained for different packing fractions η and the apex angle $2\psi = 2\pi/3$. The panel on the left is for the HB molecules while the panel on the right is for the SB molecules.

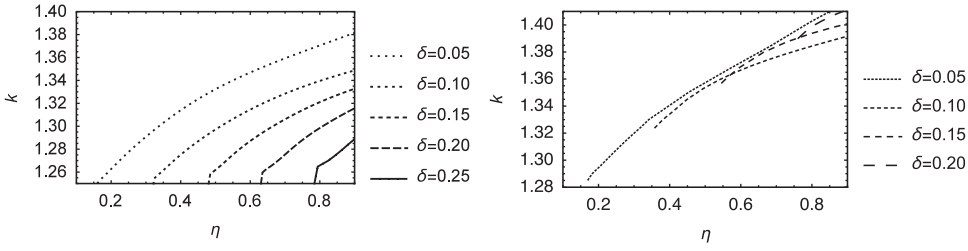

Figure 16. Equilibrium wave vector k ($k' = k/2$) in stable SmA_{AF} phase, obtained for different packing fractions and the apex angle $2\psi = 2\pi/3$ for the HB molecules (left) and for the SB molecules (right). The layer thickness is proportional to inverse of k.

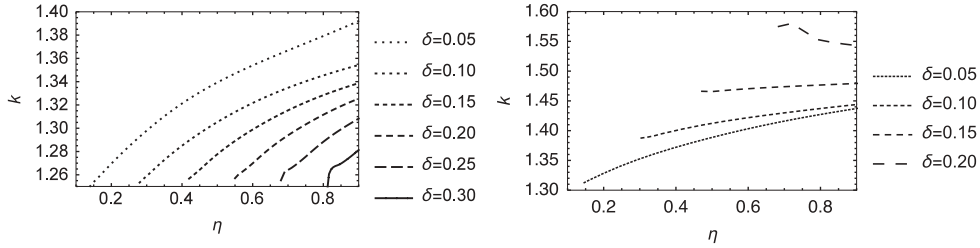

Figure 17. Equilibrium wave vector k ($k' = k/2$) in stable SmA_{AF} phase, obtained for different packing fractions and the apex angle of $2\psi = 2\pi/4$ for the HB molecules (left) and for the SB molecules (right). The layer thickness is proportional to inverse of k.

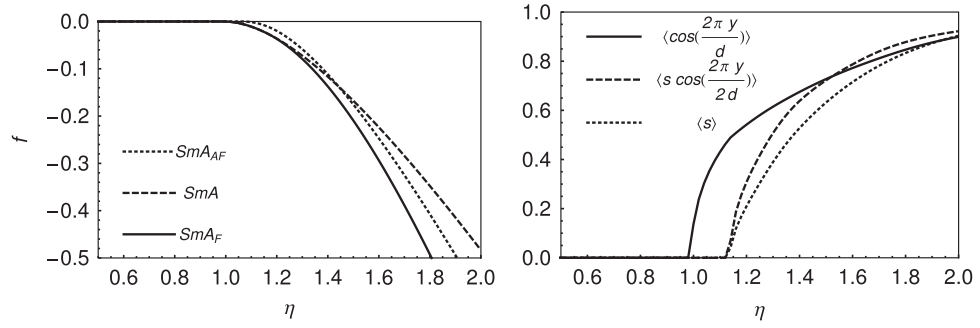

Figure 18. Dependence of free energies on packing fraction η for three structures: SmA_{AF}, SmA and SmA_F of HB system (left panel) and equilibrium, leading order parameters for stable SmA and SmA_F (right panel). Molecular parameters are $\delta = 0.4$ and $\psi = \frac{\pi}{4}$. Nematic phase ($f = 0$) is stable for $\eta < 1$ while SmA wins for $\eta > 1$. SmA_F becomes more stable than SmA for $\eta > 1.15$. Note that lamellar phases withpolarised layers are close-packed ground states for HB systems.

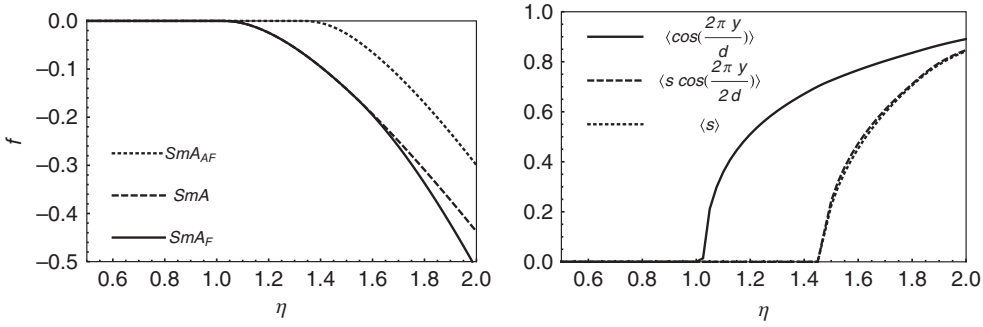

Figure 19. Dependence of free energies on packing fraction η for three structures: SmA_{AF}, SmA and SmA_F of HB system (left panel) and equilibrium, leading order parameters for stable SmA and SmA_F (right panel). Molecular parameters are $\delta = 0.5$ and $\psi = \frac{\pi}{4}$. Nematic phase ($f = 0$) is stable for $\eta < 1$ while SmA wins for $\eta > 1$. SmA_F becomes more stable than SmA for $\eta > 1.45$. Note that lamellar phases withpolarised layers are close-packed ground states for HB systems.

transition is $N - SmA$ followed by $SmA - SmA_F$ for larger ηs. The distance between both transitions grows with the width of a particle. Note that the structures became stable at high packing fractions η.

5.5. Exemplary MC simulations

In order to check whether the approximation of ideal nematic order gives correct qualitative predictions for our models, we carried out exemplary, constant pressure MC simulations for needle-like, HB and SB boomerangs. All simulations began with a set of $N = 500$ to $N = 2000$ particles of the same type, randomly oriented and placed inside a box with periodic boundary conditions applied. A single MC step involved random selection of a particle and a random translation and rotation, accepted only if the particle did not intersect with any others. N of such steps were considered as a single cycle. The size of the simulation box was dynamically adjusted to keep the pressure of the system constant. The rescaling of the box took place every 10 cycles and was successful with a probability

$$1 - \left(\frac{S_{\text{new}}}{S_{\text{old}}}\right)^{N} \exp[-p(S_{\text{new}} - S_{\text{old}}),] \tag{49}$$

if the particles in new positions did not intersect. Here, S_{old} and S_{new} denote the surface of the box before and after rescaling, respectively, and p is the pressure. These transformations were adjusted to keep the MC acceptance ratio $0.3 - 0.5$.

Exemplary snapshots taken after full equilibration of the system (10^6 cycles) are shown in Figure (20). In the panel (a), one can observe an antiferroelectric smectic phase formed by needle-like boomerangs. This is the type of smectic structure that can be observed in studied systems for the widest range of apex angles. For particles of non-zero thickness other types of smectic order can be also present, like ordinary smectic A or ferroelectric smectic. The panel (b), obtained for the HB boomerangs, corresponds to the case where domains of SmA_F order are present. The panel (c) shows, on the other hand, the SB boomerangs which are almost rod like, where two kinds of domains (smectic A and ferroelectric smectic SmA_F) coexist. The panel (d) seems to be the most spectacular one. It presents a well-ordered nematic splay-bend structure, where in the absence of positional order the ribbon-like, splay-bend modulation of orientational order emerges. In the panel (e), the splay-bend domains are observed for molecules of non-zero thickness.

It should be noted that the structures identified in simulations, along with their thermodynamic properties, agree well with predictions of density functional analysis. Even the periodicity (~10 for needle boomerangs and ~12 for the HB particles – see Figure 13) and localisation of the most disordered, splay-bend phase agree with predictions of bifurcation analysis (see the yellow region of the bifurcation diagrams, Figures (9 and 12)). It proves that orientational order limited to two discrete orientations of the steric dipole with respect to the (local) director, which we used for density functional analysis, allows for a proper identification of the structures that can condense from the nematic phase in the case of 2D hard boomerangs. However, there are also structures, which are not included in the bifurcation analysis presented, like the one in Figure (20(f)), where the molecules tend to self-organise by forming oriented rectangles, or squared blocks, without any distinguishable layered structure.

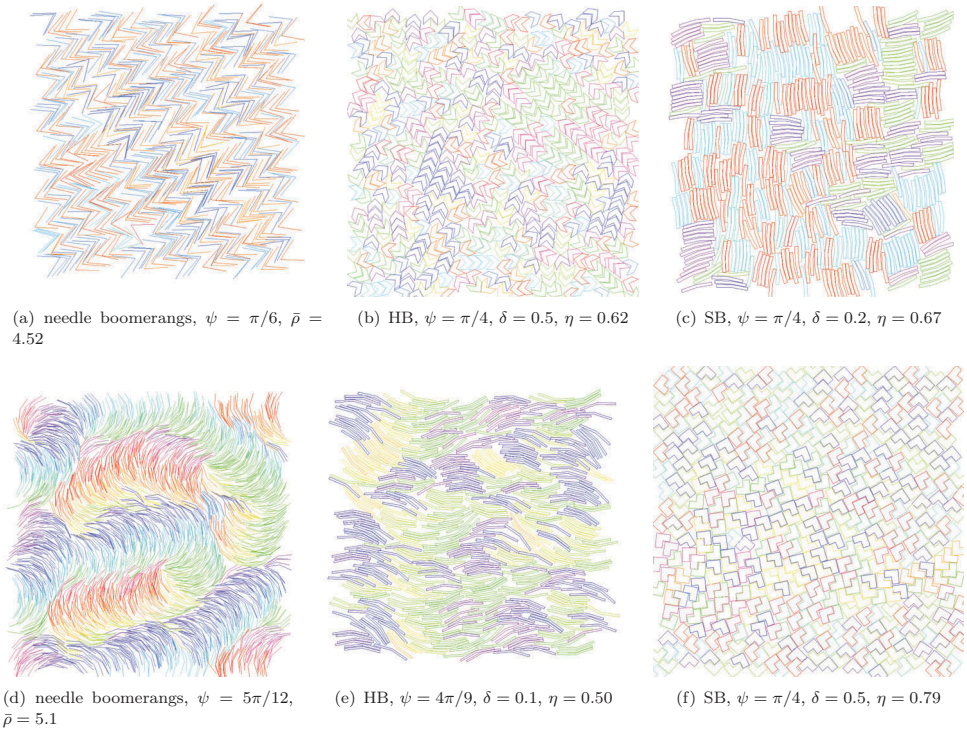

(a) needle boomerangs, $\psi = \pi/6$, $\bar{\rho} = 4.52$ (b) HB, $\psi = \pi/4$, $\delta = 0.5$, $\eta = 0.62$ (c) SB, $\psi = \pi/4$, $\delta = 0.2$, $\eta = 0.67$

(d) needle boomerangs, $\psi = 5\pi/12$, $\bar{\rho} = 5.1$ (e) HB, $\psi = 4\pi/9$, $\delta = 0.1$, $\eta = 0.50$ (f) SB, $\psi = \pi/4$, $\delta = 0.5$, $\eta = 0.79$

Figure 20. (Colour online) Exemplary snapshots from MC simulations of different particles type, apex angle ψ and width-to-length ratio δ: (a) SmA_{AF} for needle-like boomerangs; (b) SmA_F domains for boomerangs of non-zero thickness; (c) SmA and SmA_F domains; (d) nematic splay-bend for $\delta = 0$ and (e) for $\delta > 0$; (f) phase with local rectangular arrangement of bent-core molecules. Structures shown in panels (a)–(e) are consistent with the results of bifurcation analysis. At high packing fractions further structures can emerge (f) that are not included in our study. Particle parameters, like width and apex angle, are given in the panels. Colour coding is used to show different molecular orientations.

6. Summary and conclusions

We have studied 2D ensembles of bent-core-shaped molecules of zero and finite arm width, confined to the planar surface. Using the second virial Onsager DFT and the bifurcation analysis, the role of excluded volume interactions in stabilising different structures and its influence on local polarisation have been examined.

Onsager's theory reconstructs the main conclusions from [34] about the occurrence of the SmA_{AF} phase and proves that SmA_{AF} is indeed robust for 2D bent-core system. It also stays in line with the experimental observations of Gong and Wan for banana-shaped P-n-PIMB molecules absorbed onto a HOPG surface [1]. This is in spite of the fact that we disregarded any orientationally dependent interaction between substrate and molecules ($V_{ext} = 0$ in Equation (5)), limiting the role of the surface to confine the molecules in 2D (assumption of strong planar anchoring). That the surface can be considered smooth at the lengthscale of the molecular size is justified by comparing the size of bent-core P-n-PIMB molecules (a few nanometres) and the lattice spacing of HOPG (0.25 nm). Also we should add that our dimensionless shape parameter δ corresponds to $\delta \lesssim 0.2$ for P-n-PIMB.

The most interesting observation is the identification of the antiferroelectric nematic N_{SB} phase, which is stable for long bent-core molecules. This structure is foreseen from Onsager's theory and supported by exemplary, constant pressure MC simulations. To the best of our knowledge, it has not yet been reported experimentally.

We find neither smectic C nor incommensurate smectic order to become likely for these systems. We show that the actual state of the lamellar structures depend strictly on the behaviour of the Fourier transforms of the appropriately recognised parts of the excluded volume. According to this behaviour different transitions are plausible, yet phases other than antiferroelectric smectic A can be realised for a large packing fraction η. In this limit, also structures that are beyond the scope of the Onsager approach, like glassy or crystalline ones, can potentially form.

We show that small structural modifications like the change of the arm edges, the apex angle, or thickness of the arm may substantially influence the behaviour of the order parameters, wave vector and even phase diagrams. We also demonstrate that the width of the molecular arm influences the layer thickness.

The ordinary smectic A and polar smectic A phases are expected to appear at high packing fractions η, Figures (18 and 19). Since $\eta > 1$ in these cases, this raises an issue as to whether such a phase should not be excluded on the ground that Onsagers DFT is formally justified in the dilute gas limit (DGL). The reason we believe this is not the case is that the mathematically similar form of the free energy as that of Onsager's, Equations (12, 13), can be obtained by applying the Parsons-Lee (PL) rescaling/resummation technique [40–42]. They showed that the effect of (infinite) hierarchy of higher-order virial terms can be partly taken into account in (12) by an appropriate renormalisation of the second virial coefficient. Operationally, the PL rescaling replaces the second-order virial packing fraction, η, entering Equation (12) through $\bar{\rho} = \eta/S_{mol}$, by an effective packing fraction, η_{eff}, which is a monotonic function of η. The PL procedure, developed essentially for 3D systems, has been extended to 2D by Varga and Szalai [29,30]. One possibility, shown to work well, is equivalent to the replacement

$$\eta_{\text{eff}} \to \frac{1}{2}\left(\frac{\eta}{1-\eta} - \log(1-\eta)\right). \tag{50}$$

That is, the physical range of $\eta \leq 1$ is mapped on the infinite region of $\eta_{\text{eff}} \geq 0$. Assuming, for example, $\eta \lesssim 0.8$ would be equivalent to substitute $\eta_{\text{eff}} \lesssim 2.8$ in (12). Such rescaling of the free energy quantitatively improves the predictions of Onsager's theory and shifts SmA and SmA_F to lower packing fractions.

Finally, we should mention that we carried out our calculations by assuming that the reference nematic system is perfectly aligned. We considered N_{SB} along with the family of smectic states as the trial states. Therefore, some structures (like the one presented in Figure 20(f)) or phase transitions, as between smectic phases and to 2D crystalline phases, cannot be obtained using the present ansatz on one-particle density distribution function in Onsager's theory. But these structures are present at very high packing fractions, which were not taken into account in our analytical treatment. Our approximation, however, seems to work quite well as indicated by the exemplary MC simulations, which recover different smectics and even the less ordered nematic splay-bend structure.

Acknowledgements

This work was supported by Grant No. DEC-2013/11/B/ST3/04247 of the National Science Centre in Poland. The authors are also thankful to Professor Geoffrey R. Luckhurst for discussions concerning notations used for the layered structures.

Disclosure statement

No potential conflict of interest was reported by the authors.

Funding

This work was supported by the Narodowe Centrum Nauki: [Grant Number DEC-2013/11/B/ST3/04247].

References

[1] Gong J-R, Wan L-J. Two-dimensional assemblies of banana-shaped liquid crystal molecules on HOPG surface. J Phys Chem B. 2005;109:18733–18740. DOI:10.1021/jp052581q.
[2] Matharu Z, Bandodkar AJ, Gupta V, et al. Fundamentals and application of ordered molecular assemblies to affinity biosensing. Chem Soc Rev. 2012;41:1363–1402. DOI:10.1039/C1CS15145B.
[3] Niu L, Lutfor MR, Yang Y, et al. Assemblies of fluorine containing bent-shaped liquid crystal molecules studied by using scanning tunneling microscopy. J Nanosci Nanotechnol. 2010;10:7271–7276. DOI:10.1166/jnn.2010.2835.
[4] Li Y, Asik J, Yang Y, et al. Two-dimensional assemblies of banana-shaped liquid crystal molecules with short alkyl chains at solid/liquid interface. J Nanosci Nanotechnol. 2009;9:1169–1171. DOI:10.1166/jnn.2009.C112.
[5] Iglesias W, Smith TJ, Basnet PB, et al. Alignment by Langmuir/Schaefer monolayers of bent-core liquid crystals. Ferroelectrics. 2012;431:141–149. DOI:10.1080/00150193.2012.684977.
[6] Banno M, Wu Z-Q, Nagai K, et al. Two-dimensional bilayer smectic ordering of rigid rod-rod helical diblock polyisocyanides. Macromolecules. 2010;43:6553–6561. DOI:10.1021/ma1009116.
[7] Li L-S, Walda J, Manna L, et al. Semiconductor nanorod liquid crystals. Nano Lett. 2002;2:557–560. DOI:10.1021/nl0255146.
[8] Querner C, Fischbein MD, Heiney PA, et al. Millimeter-scale assembly of CdSe nanorods into smectic superstructures by solvent drying kinetics. Adv Mat. 2008;20:2308–2314. (and references therein). DOI:10.1002/adma.200800125
[9] Jákli A. Liquid crystals of the twenty-first century nematic phase of bent-core molecules. Liq Cryst Rev. 2013;1:65–82. DOI:10.1080/21680396.2013.803701.
[10] Takezoe H, Takanishi Y. Bent-core liquid crystals: their mysterious and attractive world. Jap J App Phys. 2006;45:597–625. DOI:10.1143/JJAP.45.597.
[11] Borshch V, Kim Y-K, Xiang J, et al. Nematic twist-bend phase with nanoscale modulation of molecular orientation. Nat Commun. 2013;4:2635.
[12] Chen D, Porada JH, Hooper JB, et al. Chiral heliconical ground state of nanoscale pitch in a nematic liquid crystal of achiral molecular dimers. Proc Nat Acad Sci. 2013;110:15931–15936. DOI:10.1073/pnas.1314654110.
[13] Tamba MG, Salili SH, Zhang G, et al. A fibre forming smectic twist-bent liquid crystalline phase. RSC Adv. 2015;5:11207–11211. DOI:10.1039/C4RA14669G.
[14] Francescangeli O, Vita F, Samulski ET. The cybotactic nematic phase of bent-core mesogens: state of the art and future developments. Soft Mat. 2014;10:7685–7691. DOI:10.1039/C4SM01256A.
[15] Grzybowski P, Longa L. Biaxial nematic phase in model bent-core systems. Phys Rev Lett. 2011;107:027802. DOI:10.1103/PhysRevLett.107.027802.
[16] Meyer RB. Structural problems in liquid crystal physics. In: Balian R, Weil G, editors. Les Houches summer school in theoretical physics, 1973. Molecular fluids. New York: Gordon and Breach; 1976. p. 273.
[17] Dozov I. On the spontaneous symmetry breaking in the mesophases of achiral banana-shaped molecules. Europhys Lett. 2001;56:247–253. DOI:10.1209/epl/i2001-00513-x.
[18] Shamid SM, Dhakal S, Selinger JV. Statistical mechanics of bend flexoelectricity and the twist-bend phase in bent-core liquid crystals. Phys Rev E. 2013;87:052503–11. DOI:10.1103/PhysRevE.87.052503.
[19] Longa L, Pająk G. Modulated nematic structures induced by chirality and steric polarization. Phys Rev E. 2016;93:040701(R)-5. DOI:10.1103/PhysRevE.93.040701.
[20] Lubensky TC, Radzihovsky L. Theory of bent-core liquid-crystal phases and phase transitions. Phys Rev E. 2002;66:031704–27. DOI:10.1103/PhysRevE.66.031704.
[21] Longa L, Pająk G, Wydro T. Chiral symmetry breaking in bent-core liquid crystals. Phys Rev E. 2009;79:040701(R)-4. DOI:10.1103/PhysRevE.79.040701.
[22] Trojanowski K, Pająk G, Longa L, et al. Tetrahedratic mesophases, chiral order, and helical domains induced by quadrupolar and octupolar interactions. Phys Rev E. 2012;86:011704–011713. DOI:10.1103/PhysRevE.86.011704.
[23] Longa L, Trojanowski K. Ambidextrous chiral domains in nonchiral liquid-crystalline materials. Act Phys Polon B. 2013;44:1201–1208. DOI:10.5506/APhysPolB.44.1201.
[24] Kunz H, Zumbach G. Topological phase transition in a two-dimensional nematic n-vector model: A numerical study. Phys Rev B. 1992;46:662–673. DOI:10.1103/PhysRevB.46.662.
[25] Frenkel D, Eppenga R. Evidence for algebraic orientational order in a two-dimensional hard-core nematic. Phys Rev. 1985;31:1776–1787. DOI:10.1103/PhysRevA.31.1776.
[26] Vink RLC. The isotropic-to-nematic transition in a two-dimensional fluid of hard needles: a finite-size scaling study. Eur Phys J B. 2009;72:225–231. DOI:10.1140/epjb/e2009-00333-x.
[27] Bates MA, Frenkel D. Phase behavior of two-dimensional hard rod fluids. J Chem Phys. 2000;112:10034–10041. DOI:10.1063/1.481637.
[28] Tavarone R, Charbonneau P, Stark H. Phase ordering of zig-zag and bow-shaped hard needles in two dimensions. J Chem Phys. 2015;143:114505–114513. DOI:10.1063/1.4930886.
[29] Varga S, Szalai I. Phase transitions of hard ellipses and hard ellipses with circular square-wells based upon density functional theory. Mol Phys. 1998;95:515–523. DOI:10.1080/00268979809483186.
[30] Varga S, Szalai I. Parsons-Lee theory and a simulation-based study of two-dimensional hard-body fluids. J Mol Liq. 2000;85:11–21. DOI:10.1016/S0167-7322(99)00160-9.

[31] Chrzanowska A. On the application of the Onsager DFT theory to two-dimensional system of hard needles. Act Phys Polon B. 2005;36:3163–3178.
[32] Chrzanowska A. Bifurcation analysis of a two-dimensional binary mixture of hard needles. Act Phys Polon B. 2013;44:91–106. DOI:10.5506/APhysPolB.44.91.
[33] Bisi F, Rosso R, Virga EG, et al. Polar steric interactions for V-shaped molecules. Phys Rev E. 2008;78:011705–011708. DOI:10.1103/PhysRevE.78.011705.
[34] Martínez-González JA, Varga S, Gurin P, et al. Spontaneously bended nematic and antiferroelectric smectic structures of banana-shaped hard particles in two dimensions. EPL. 2012;97:26004–p6. DOI:10.1209/0295-5075/97/26004.
[35] Martínez-González JA, Varga S, Gurin P, et al. Structural properties of hockey stick-shaped particles in two dimensions. J Mol Liq. 2013;185:26–31. DOI:10.1016/j.molliq.2012.11.020.
[36] Martínez-Ratón Y, Velasco E, Mederos L. Demixing behavior in two-dimensional mixtures of anisotropic hard bodies. Phys Rev E. 2005;72:031703–031711. DOI:10.1103/PhysRevE.72.031703.
[37] Varga S, Gurin P, Armas-Pérez JC, et al. Nematic and smectic ordering in a system of two-dimensional hard zigzag particles. J Chem Phys. 2009;131:184901–184910. DOI:10.1063/1.3258858.
[38] Evans R. The nature of the liquid-vapour interface and other topics in the statistical mechanics of non-uniform, classical fluids. Adv Phys. 1979;28:143–200. DOI:10.1080/00018737900101365.
[39] Longa L, Grzybowski P, Romano S, et al. Minimal coupling model of the biaxial nematic phase. Phys Rev E. 2005;71:051714–13. DOI:10.1103/PhysRevE.71.051714.
[40] Parsons JD. Nematic ordering in a system of rods. Phys Rev. 1979;19:1225–1230. DOI:10.1103/PhysRevA.19.1225.
[41] Lee SD. A numerical investigation of nematic ordering based on a simple hard rod model. J Chem Phys. 1987;87:4972–4974. DOI:10.1063/1.452811.
[42] Lee SD. The Onsager type theory for nematic ordering of finite length hard ellipsoids. J Chem Phys. 1988;89:7036–7037. DOI:10.1063/1.455332.

Appendix

We add here, for completeness, the formulae for the Fourier transforms of the interaction-excluded slice kernel for the SB boomerangs discussed in Section V. Subscripts refer to coefficients calculated for cases shown in Figure (10).

$$\begin{aligned}\alpha_I(\psi,\delta,k) = \tfrac{1}{8k^2}\quad & [4\sec^2(\psi)\cos(2k(\delta\cot(\psi)-1))\cos^2(k-\delta k\cot(\psi))\\ & +\cos(2\psi)\sec^2(\psi)\cos(2\delta k\cot(\psi))-2\cos(k(\delta\csc(\psi)\sec(\psi)-2))\\ & +2\cos(2k)\cos(2\psi)\sec^2(\psi)-\cos(4k)(\sec^2(\psi)+2)-2]\end{aligned} \tag{51}$$

$$\begin{aligned}\alpha_{II}(\psi,\delta,k) = \tfrac{1}{8k^2}\quad & \{-\tan(\psi)\csc(2\psi)[2\cos(4k\cos^2(\psi)(\delta\cot(\psi)-1))\\ & -4\cos(2k(\delta\cot(\psi)-1))-2\cos(4k(\delta\cot(\psi)-1))+\cos(4k-2\psi)\\ & -2\cos(2(k-\psi))-2\cos(2(k+\psi))+\cos(2(2k+\psi))\\ & +4\cos(4k)+2\cos(2\psi)]\}\end{aligned} \tag{52}$$

$$\begin{aligned}\alpha_{III}(\psi,\delta,k) = \tfrac{1}{8k^2}\quad & [\sec^2(\psi)(2\cos^2(\psi)\cos(2k(\delta\cot(\psi)-1))-2\cos(2\psi)\cos(2k(\delta\cot(\psi)-2))\\ & +\cos(4k(\delta\cot(\psi)-1))+\cos(4k)(\cos(2\psi)-2))]\end{aligned} \tag{53}$$

$$\begin{aligned}\beta_I(\psi,\delta,k) = \tfrac{1}{8k^2}\quad & [(\sec^2(\psi)-2)\cos(2\delta k\cot(\psi))+2(\cos(k(2-\delta\csc(\psi)\sec(\psi)))\\ & +\sec^2(\psi)(2\cos(2k(\delta\cot(\psi)-1))\sin^2(k-\delta k\cot(\psi))\\ & +\cos(2k)\cos(2\psi))-1)+\cos(4k)(\sec^2(\psi)-2)]\end{aligned} \tag{54}$$

$$\begin{aligned}\beta_{II}(\psi,\delta,k) = -\tfrac{1}{16k^2}\quad & [\sec^2(\psi)(-2\cos(4k\cos^2(\psi)(\delta\cot(\psi)-1))-4\cos(2k(\delta\cot(\psi)-1))\\ & +2\cos(4k(\delta\cot(\psi)-1))+\cos(4k-2\psi)-2\cos(2(k-\psi))\\ & -2\cos(2(k+\psi))+\cos(2(2k+\psi))+2\cos(2\psi)+4)]\end{aligned} \tag{55}$$

$$\begin{aligned}\beta_{III}(\psi,\delta,k) = \tfrac{1}{8k^2}\quad & [\sec^2(\psi)(6\cos^2(\psi)\cos(2k(\delta\cot(\psi)-1))\\ & +\cos(2\psi)(\cos(4k)-4\cos^2(k(\delta\cot(\psi)-2)))\\ & -\cos(4k(\delta\cot(\psi)-1))-2)]\end{aligned} \tag{56}$$

$$\beta_I(\psi,\delta,k\to 0) = \tfrac{1}{4}\csc(2\psi)\left(6\delta^2\cos(2\psi)+\left(\delta^2-1\right)\cos(4\psi)+3\delta^2-4\delta\sin(2\psi)+1\right) \tag{57}$$

$$\beta_{II}(\psi,\delta,k\to 0) = \tfrac{1}{2}\sec^2(\psi)\left((\delta\cot(\psi)-1)^2-2\cos^2(\psi)\cot^2(\psi)(\sin(\psi)-\delta\cos(\psi))^2+\cos(2\psi)\right) \tag{58}$$

$$\beta_{III}(\psi,\delta,k\to 0) = \tfrac{1}{2}\left(\delta^2-2\delta\cot(\psi)+1\right) \tag{59}$$